Macromolecules

Article

Cite This: Macromolecules XXXX, XXX, XXX−XXX

UV- and Thermo-Controllable Azobenzene-Decorated Polycarbodiimide Molecular Springs

Dumindika A. Siriwardane,*[,†] Oleg Kulikov,[‡] Benjamin L. Batchelor,[†] Zhiwei Liu,[§] John Michael Cue,[†] Steven O. Nielsen,[†] and Bruce M. Novak*[,†]

[†]Department of Chemistry and Biochemistry, The University of Texas at Dallas, Richardson, Texas 75080, United States

[‡]Department of Chemistry, Massachusetts Institute of Technology, 77 Massachusetts Ave., Cambridge, Massachusetts 02139, United States

[§]Department of Chemistry and Biochemistry, University of the Sciences, 600 South 43rd Street, Philadelphia, Pennsylvania 19104, United States

Supporting Information

ABSTRACT: Molecular switches offer wide applicability through conformational changes which can be triggered by external stimuli. Azobenzenes are excellent candidates to contribute toward a rational design of molecular switches because they exist as either *cis* or *trans* isomers as a result of the dynamic photoisomerization process. In this study, we leverage the azobenzene stimuli response by attaching it as a pendant group on polycarbodiimides synthesized using screw sense polymerization. The exposure of the polymer sample in solution to UV light induces the transformation of the azobenzene pendant groups to the *cis* isomer with re-emergence of the *trans* conformer under visible light or heat. Corroborating experimental and computational data reveal that these events induce spring-like expansion−contraction motions throughout the helical backbone. Our finding suggests the use of polycarbodiimide-derived photoswitches as dynamic materials in biological applications and materials science.

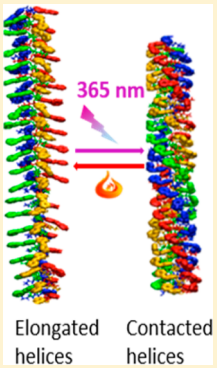

INTRODUCTION

The design of molecular switches showing bistability in response to an external stimuli, such as solvent,[1] pH,[2] ions,[3] and temperature,[4] has been a growing area of interest. The presence of two specific molecular conformations that can be precisely controlled is an important strategy for the creation of molecular switches. By employing bistability, various polymeric systems have been designed for specific functions. These systems are capable of controlling a specific event selectively upon triggering with light,[5] solvent,[6,7] pH,[8] or temperature,[9] providing advantages toward chiral separation,[10] polymeric liquid crystalline materials,[11−13] chiral support,[14] and *in vivo* drug delivery studies.[15]

Synthesis of artificial helical systems is an emerging area of polymer chemistry due to its diverse applications such as chiroptical switches,[16] reconfiguring emulsions,[17] drug delivery agents,[18] and optoelectronics.[19] With regard to helical polymers such as polycarbodiimides and polyisocyanates, the helical inversions between *P* and *M* helices,[20] helix-to-coil,[21] coil−helix transitions,[22,23] and helical expansion−contractions (helical breathing) are promising and practical areas of research as these undergo molecular level dynamic assemblies which are essential for molecular switches. We have extensively studied the chiroptical switching behavior of polycarbodiimides capable of exhibiting conformational changes with respect to solvent and temperature. For instance, poly(*N*-naphthyl-*N*′-octadecylcarbodiimide) shows temperature- and solvent-induced chiroptical switching behavior. These changes occur due to the reversible shutter-like reorientation of naphthalene scaffolds through imine inversion.[16] This unique reorientation causes the polymer backbone to undergo changes in helical pitch as evident by VCD (vibrational circular dichroism) and DFT (density functional theory) calculations.

Inspired by these results, in this study we investigated how photochemical and thermal isomerization of azobenzene pendant groups influences the polymer helicity. The discovery of azobenzene systems as photoswitches is one of the milestones in photochemistry as it shows isomerization between *trans* and *cis* forms upon UV irradiation. The azobenzene motif has been incorporated into various types of molecules including virus-based nanowires,[24] peptides,[25] proteins,[26] nucleic acids, and ion channels[27] for spatial and temporal control of various activities which rely on reversible conformational changes upon illumination of the azo chromophore. For instance, Wooley and co-workers reported an elegant azobenzene-based photoswitch linked to peptides to regulate their affinity toward DNA binding via photoisomerization.[28]

In this work, our specific goal was to understand the chiroptical switching behavior of the polycarbodiimide backbone occurring through isomerization of azobenzene pendant

Received: March 30, 2018
Revised: May 1, 2018

DOI: 10.1021/acs.macromol.8b00679
Macromolecules XXXX, XXX, XXX−XXX

scaffolds in poly(*N*-(1,2-diphenyldiazene)-*N*′-hexylcarbodiimide) of both *R*- and *S*-configurations.

MATERIALS AND METHODS

Chemicals for the synthesis of all monomers were purchased from Sigma-Aldrich (Milwaukee, WI) and used as received unless stated otherwise. The certified ACS grade solvents were purchased from Fisher Scientific and distilled prior to use. Column chromatography on monomers was performed by using neutral high purity silica gel. All monomers and polymers were stored in an N_2 atmosphere MBraun UNILAB glovebox prior to use.

^{1}H NMR and ^{13}C NMR were recorded using a Bruker Advance III 500 MHz NMR spectrometer at room temperature. Specific optical rotation (SOR) data were recorded on a JASCO P-1010 polarimeter at λ = 589 nm and at a sample concentration of 2.0 mg/mL by using a 100 mm path length cell. Solution-state vibrational circular dichroism (VCD) spectra were obtained on a Bio Tool Chiral-2X VCD spectrometer by dissolving samples in deuterated toluene (C = 25 mg/mL and l = 50 μm). A Raguku Ultima III X-ray diffractometer was used to record all *p*-XRD profiles of powder samples. Tapping mode atomic force microscopy (TM-AFM) was performed by using a Nanoscope IV Multimode Veeco instrument on silicon wafers (diameter, d = 2.5 cm, Wafer World). All imaging was performed at room temperature with a silicon cantilever with a nominal constant of 42 N/m and 320 kHz using an OTESPA tip. Scanning electron microscopy (SEM) imaging was done by using a Zeiss Supra 40 instrument. The samples were mounted on a silicon wafer and coated with a conductive Pd/Au film. The potential applied to the inspection sample was 10 keV. Size exclusion chromatography (SEC) was performed on a Viscotek VE 3580 system equipped with ViscoGel columns (GMHHR-M), connected to a refractive index detector to determine the polymer molar masses.

Synthesis of *N*-(1,2-Diphenyldiazene)-*N*′-hexylurea. First, 5.000 g (1 equiv, 39.3 mmol) of hexyl isocyanate was dissolved in 150 mL of $CHCl_3$ in a 250 mL round-bottom flask and cooled in an ice bath. Then, 7.751 g (1 equiv, 39.3 mmol) of 4-aminoazobenzene was added dropwise while stirring. The mixture was refluxed at 60 °C overnight. At the end of the reaction time, the solvent was evaporated, and the product was obtained as a red solid. It was recrystallized from hot ethanol and dried under vacuum overnight.

Yield = 10.320 g (81%, red needle-like short crystals); ^{1}H NMR (500 MHz, $CDCl_3$, δ ppm): 7.91−7.43 (overlapped multiplets, 9H, Ar−H), 6.57 (br, 1H, Ar−N−H), 4.80 (br, 1H, C−N−H), 3.30, 3.29, 3.27, 3.26 (q, 2H, N−CH_2), 1.57−1.25 (overlapped multiplet, 8H, alkane H), 0.90, 0.89, 0.87 (t, 3H, terminal CH_3); ^{13}C NMR (126 MHz, $CDCl_3$, δ ppm): 155.04 (C═O, amide carbonyl), 152.87 (C−N═N), 148.53 (C−N═N), 141.73 (C−NH), 130.73, 129.19, 124.39, 122.81, 119.81(Ar C═C), 40.76 (NH−CH_2), 31.65, 30.17, 26.72, 22.72 (hexyl chain CH_2), 14.17 (terminal CH_3).

Synthesis of *N*-(1,2-Diphenyldiazene)-*N*′-hexylcarbodiimide Monomer. 13.031 g (1.25 equiv, 30.8 mmol) of PPh_3Br_2 was placed in cold DCM. Then 8.6 mL, (2.5 equiv, 61.6 mmol) of triethylamine was added dropwise under nitrogen. The mixture was stirred for 10 min. Then 8.101 g (1 equiv, 24.6 mmol) of urea was added slowly while stirring. After stirring for 1 h at room temperature, the ice bath was removed, and an excess of hexanes was added. The precipitated solid was filtered and discarded. The monomer was extracted into hexanes and purified using a SiO_2 column with DCM as the eluent. Yield = 6.32 g (86%, clear red oil). ^{1}H NMR (500 MHz, $CDCl_3$, δ ppm): 7.91−7.19 (overlapped multiplets, 9H, Ar−H), 3.48, 3.47, 3.46, (t, 2H, N−CH_2), 1.74−1.31 (m, overlapped, 8 H, alkanes), 0.92, 0.90, 0.89 (t, 3H, CH_3). ^{13}C NMR (126 MHz, $CDCl_3$, δ ppm): 152.70 (C−N═N), 149.50 (N═C═N, carbodiimide), 144.11, 134.31, 130.77 (C−N), 129.08, 124.22, 124.02, 122.74, 120.16 (Ar C═C), 46.87 (N−CH_2), 31.27, 26.47, 22.55, 14.01 (C−H, alkanes).

Synthesis of Poly(*N*-(1,2-diphenyldiazene)-*N*′-hexylcarbodiimide), P-1. To synthesize (*R*)- and (*S*)-polymers, (*R*)-BINOL-Ti(IV) and (*S*)-BINOL-Ti(IV) initiators were used, respectively. The monomer to initiator ratio was 250:1. Inside the glovebox, 1.502 g (250 equiv, 4.9 mmol) of monomer was placed in an oven-dried sample vial along with 1.0 mL of $CHCl_3$. Then, 8.8 mg (1 equiv, 19.6 μmol) of (*S*)- or (*R*)-initiator was added and stirred overnight. At the end of the reaction time, material from the vial was dissolved in $CHCl_3$, precipitated from MeOH three times, and then dried under vacuum for 2 days. For (*S*)-**P-1**: yield = 1.101 g (73%); $^{21}[\alpha]_{589}$ = −273°, M_n = 21 000 Da. ^{1}H NMR (500 MHz, $CDCl_3$, δ ppm): 7.71−6.54 (br, Ar H), 3.59−2.63 (br, N−CH_2), 1.58−0.41 (br, alkanes). ^{13}C NMR (126 MHz, $CDCl_3$, δ ppm): 152.87 (C−N═N), 150.24 (C═N, imine), 148.45, 147.71, 130.25, 129.06 (C−N), 128.76, 123.93, 123.76, 122.53, 119.87 (Ar C═C), 47.40 (N−CH_2), 31.45, 29.64, 28.21, 26.15, 22.35, 13.62 (C−H, alkanes). For (*R*)-**P-1**: yield = 1.321 g (88%); $^{21}[\alpha]_{589}$ = 305°, M_n = 22 500 Da.

Synthesis of Poly(*N*-(1,2-diphenyldiazene)-*N*′-hexylcarbodiimide)-*random*-poly(*N*-phenethyl-*N*′-methylcarbodiimide), P-2. Inside the glovebox, 0.500 g (250 equiv, 16.3 mmol) of *N*-(1,2-diphenyldiazene)-*N*′-hexylcarbodiimide and 26.1 mg (25 equiv, 1.6 mmol) of *N*-phenethyl-*N*′-methylcarbodiimide monomers were placed along with 1.0 mL of $CHCl_3$. Then, 2.9 mg (1 equiv, 6.5 μmol) of (*RAC*)-BINOL-Ti(IV) initiator was added and stirred for 18 h. At the end of the reaction time, the gelled polymer was dissolved in $CHCl_3$ and precipitated from MeOH three times. The product was dried under vacuum for 2 days. Yield = 0.44 g (84%); $^{21}[\alpha]_{589}$ = −113°, M_n = 20 300 Da. ^{1}H NMR (500 MHz, $CDCl_3$, δ ppm): 7.89, 7.76, 7.42, 7.26, 7.01, 6.86 (br, overlapped, Ar−H), 5.94, 5.39, 5.06 (br, methine H from PPEMC), 3.69, 3.66 (br, amine N−CH_2), 3.27, 3.24 (br, N−CH_3), 2.67 (br, amine N−CH_2), 1.65, 1.30, 0.88, 0.74, 0.55, 0.47 (alkanes, CH_2 and CH_3). ^{13}C NMR (126 MHz, $CDCl_3$, δ ppm): 152.95 (C−N═N), 150.54 (imine, C═N), 148.41 (imine, C═N), 130.77−119.58 (Ar C═C), 47.54 (methine C, C−H), 32.15, 28.68, 27.04, 22.97, 14.17 (alkanes, CH_2 and CH_3).

Synthesis of Poly(*N*-(1,2-diphenyldiazene)-*N*′-hexylcarbodiimide)-*random*-poly(*N*-phenethyl-*N*′-methylcarbodiimide), P-3. The same procedure was carried out for **P-3** with 0.503 g (1 equiv, 1.6 mmol) of *N*-(1,2-diphenyldiazene)-*N*′-hexylcarbodiimide, 0.261 g (1 equiv, 1.6 mmol) of *N*-phenethyl-*N*′-methylcarbodiimide, and 23.1 mg of (*RAC*)-BINOL-Ti(IV) initiator. Yield = 0.65 g (85%); $^{21}[\alpha]_{589}$ = −156°, M_n = 20 150 Da. ^{1}H NMR (500 MHz, $CDCl_3$, δ ppm): 7.91, 7.90, 7.51, 7.47, 7.36 (br, overlapped, Ar−H), 4.98, 4.59 (br, methine H, C−H), 3.25, 2.74 (br, overlapped, N−CH_3 and N−CH_2), 1.81, 1.64, 1.30, 0.90, 0.12 (br, overlapped, CH_2 and CH_3, alkanes). ^{13}C NMR (126 MHz, $CDCl_3$, δ ppm): 152.84 (C−N═N), 147.77 (imine C═N), 129.52, 128.78, 127.99, 126.21, 122.89, 122.50 (Ar C═C), 34.72 (amine N−CH_3), 31.46, 26.69, 22.24, 14.18 (alkanes, CH_2 and CH_3).

Molecular Dynamic Simulation Methods. All simulations were run using the NAMD software package[29] with the following parameter choices: temperature 293 K enforced with a Langevin thermostat with damping parameter 1.0 ps^{-1}; cutoff distance 12 Å for the van der Waals interactions and the changeover from real space to reciprocal space for the electrostatic interactions; time step 0.5 fs; particle mesh Ewald (PME) grid spacing of 1 Å. For the vacuum simulations, periodic boundary conditions were not used, and therefore PME was not needed.

In addition, in all simulations, a weak harmonic constraint, with force constant 0.25 kcal mol^{-1} Å^{-2}, was applied to the y and z coordinates of the carbon and nitrogen atoms of the polymer backbone (namely one carbon and one nitrogen atom per monomer) in order to keep the backbone aligned with the x-axis. This constraint was used primarily to facilitate analysis; simulations run without the constraint showed only minor deviations of the polymer backbone from a straight line.

The MD simulations used a fully atomistic force field as follows. First, all force field parameters except those for chloroform were obtained from CGenFF[30,31] using the online server at https://cgenff.paramchem.org. Second, the azobenzene parameters were modified[32] and further modified as described in Figure S11.[33] Last, the chloroform parameters of ref 33 were used; the van der Waals cross-interactions for this chloroform model do not follow the Lorentz−Berthelot combination rules and instead are implemented using the "nbfix" command.

DOI: 10.1021/acs.macromol.8b00679
Macromolecules XXXX, XXX, XXX−XXX

All production simulations were run for 50 ns, corresponding to 1×10^8 time steps. The vacuum simulations consisted of one 80-mer, which has 3612 atoms. The chloroform simulations consisted of one 80-mer and roughly 2100 chloroform molecules for a total of roughly 14 000 atoms (the exact number varied from system to system). For the chloroform simulations, periodic boundary conditions were used. Each system in Table 1 was run for at least 2×10^8 time steps prior to the production run. For the systems in panel B of Figure 4, corresponding to the E-H states of Table 1, the initial condition was taken from the production run of the opposite *cis*/*trans* conformation and instantaneously switched to the correct conformation using the appropriate single-minimum torsion potential of Figure S11. Once the correct conformation is obtained, it makes no difference whether the torsion potential is left as is (namely as the appropriate single-minimum curve of Figure S11) or changed back to the double-minimum curve (labeled "original" is Figure S11). In each simulation, all 80 monomers of the 80-mer have the same *cis*/*trans* conformation.

Table 1. Summary of the MD Simulations Performed for the 80-mer under Different Conditions[a]

	cis/*trans*	initial length of the 80-mer	environment	end-to-end length (nm)	total rotation (deg)	SASA/length (nm)
A	*trans*	long	vacuum	16.8	+72	13.1
B	*cis*	short	vacuum	14.4	−436	10.3
C	*trans*	long	$CHCl_3$	17.0	+72	13.5
D	*cis*	short	$CHCl_3$	14.6	−336	10.6
E (from B)	*trans*	short	vacuum	16.8	+79	13.1
F (from A)	*cis*	long	vacuum	14.3	−470	10.3
G (from D)	*trans*	short	$CHCl_3$	16.8	+36	13.6
H (from C)	*cis*	long	$CHCl_3$	16.9	+47	10.6

[a]Each simulation was run for 50 ns. The reported data is the average over the stable portion of the run (Figure 4).

The last column of Table 1 is calculated as follows. The default solvent accessible surface area (SASA) algorithm implemented in VMD is used to compute the SASA of the 80-mer.[34] Then this value is divided by the 80-mer average length (Table 1). Since the surface area of a cylinder is πdL with d the diameter and L the length, the SASA/length value can be interpreted as the circumference (πd) of the polymer cross section.

The total rotation angle of Table 1 is calculated according to

$$\frac{1}{4}\sum_{j=0}^{3}\sum_{i=2}^{20}\Delta\theta(4(i-1)-j, 4i-j)$$

In this formula, the sum of the rotation angles $\Delta\theta$ between monomers i and $i + 4$ is computed for the 80-mer and averaged over the four different j values, with each j value corresponding to a different color in Figure 3. Since the polymer backbone lies on the x-axis, we compute $\Delta\theta(a,b)$ between monomers a and b as follows. The y and z coordinate values of the first azobenzene carbon atom (in terms of the bonds connecting the azobenzene unit to the polymer backbone) are used to compute the angles $\theta(a) = \tan^{-1}(z_a/y_a)$ and $\theta(b) = \tan^{-1}(z_b/y_b)$. Then $\Delta\theta(a,b) = \theta(b) - \theta(a)$.

Density Functional Calculations. To corroborate experimental IR spectra and conformational results from MD simulations, we carried out density functional theory (DFT) calculations on eight model octamers. For each *cis* or *trans* state, we chose four different octameric fragments from an 80-mer conformation of the MD simulation. The hexyl chains were then shorted to ethyl and appropriate terminal groups ($-OCH_3$ and $-H$) added. Geometry optimization and IR spectra calculations were then carried out at the B3LYP/6-31G level of theory, using the Gaussian 09 software package.[35] Implicit solvation was applied by the integral equation formalism polarizable continuum model (IEFPCM)[36] for chloroform. The IR spectra were generated using a scaling factor of 0.975.

UV−Vis Experiment. 4.1 mg of (*S*)-**P-1**, **P-2**, and **P-3** was dissolved in 50.0 mL of $CHCl_3$. The UV−vis spectra were recorded after 10 min of irradiation with a UV 365 nm source.

SOR Experiment. 2.0 mg/mL solutions of both (*S*)- and (*R*)-**P-1** were prepared, and SOR was measured at λ = 589 nm upon UV irradiation for 1 h. Then, the samples were annealed at 40 °C, and SOR was recorded again until it showed a constant value.

TM-AFM Imaging. 4.0 mg/mL solutions were prepared for **P-1**, **P-2**, and **P-3** polymers in $C_2H_2Cl_4$ (1,1,2,2-tetrachloroethane), and two sets of samples were drop-casted on silicon wafer separately. Then one set of samples was exposed to UV 365 nm radiation for 18 h. Thin film morphology was studied by TM-AFM.

Solid-State FTIR Studies. For the FTIR studies, 10.0 mg of (*S*)-**P-1** was used. Differential scanning calorimetry (DSC) was performed on a Mettler Toledo DSC-1 using a temperature range from −20 to 160 °C at a rate of 10 °C/min and also from −20 to 200 °C at a rate of 10 °C/min, interrupting the run at multiple temperatures (i.e., −25, 10, 20, 40, 60, and 80 °C). The samples were then immediately tested on a Shimadzu IRAffinity-1 Fourier transform infrared (FTIR) spectrometer using the Pike MIRacle attenuated total reflectance (ATR) attachment. Poly(*N*-phenyl-*N*′-hexylcarbodiimide) was used as a control.

DISCUSSION

Incorporation of different functionalities into helical backbones has become a powerful tool in the synthesis of functional, helical polymers. The enhanced diversity through incorporation of modifiable groups in this unique polymeric architecture leads to intriguing properties.[37,38] Polycarbodiimides are helical polymers composed of a nitrogen-rich, rigid-amidine backbone along with two tunable pendant groups. In our previous work, we investigated the chiroptical switching behavior of polycarbodiimides which have been decorated with anthracene and naphthylarene pendants in a regioregular fashion to yield poly(*N*-anthracene-*N*′-octadecyl)carbodiimides (PAOD) and poly(*N*-naphthyl-*N*′-octadecylcarbodiimides) (PNOC), respectively.[16,39] The IR spectra of PNOC in various solvents show variations of two distinct imine stretching modes at 1621 and 1640 cm^{-1} providing evidence for the switching behavior of the helical backbone. As the specific optical rotation increases depending on the solvent employed, we observed variations in the intensity of these two modes with simultaneous variations detected upon changing the temperature of PNOC solutions in THF. This suggested that the chiroptical switching process is caused by changes in the populations of two distinct conformations.

In this work, we report the synthesis of polycarbodiimides which are decorated with azobenzene photochromic groups at the imine positions. These azobenzene derivatives are promising candidates for molecular switches as the conformational changes are reversible. To explore the feasibility of chiroptical switching behavior, azobenzene appended helical polycarbodiimides have been synthesized by using an achiral monomer of *N*-(1,2-diphenyldiazene)-*N*′-hexylcarbodiimide (**M-1**) (Schemes 1 and 2). Through the reversible coordination−insertion polymerization mechanism with chiral (*R*)- and (*S*)-BINOL-Ti(IV) initiators, excess helical sense polymers were obtained exhibiting SOR values at +290° for (*R*)-screw sense and −289° for (*S*)-screw sense of **P-1**, respectively.

We have also utilized racemic (*RAC*)-BINOL-Ti(IV) initiator to synthesize azo-decorated polycarbodiimide, and the screw sense has been induced via the sergeants-and-soldiers effect.[40] To validate the screw sense, 10 mol % of the chiral stimulant of (*R*)-*N*-methyl-*N*′-phenethylcarbodiimide (**M-2**) was used. The main reason for synthesis of **P-2** and **P-3** is incorporation of handedness into the polymer system with a

DOI: 10.1021/acs.macromol.8b00679
Macromolecules XXXX, XXX, XXX−XXX

Scheme 1. Synthesis of Urea and Its Respective Carbodiimide Monomer

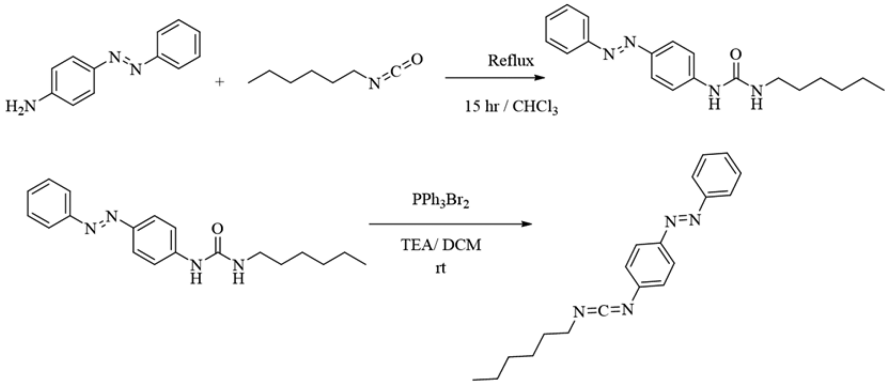

Scheme 2. Synthesis of Azo-Decorated Polycarbodiimides

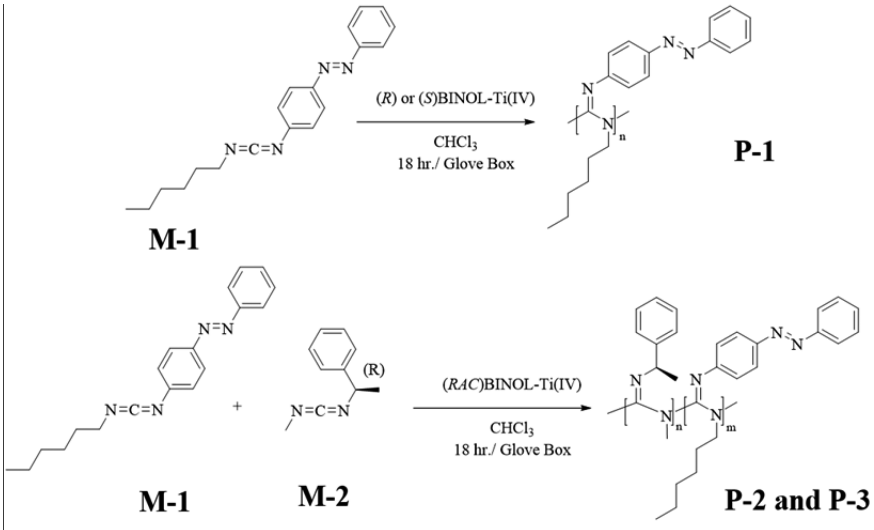

Polymer	n (mol%)	m (mol%)
P-1	0	100
P-2	10	90
P-3	50	50

chiral stimulant which possesses an asymmetric center. We investigated the change of **P-2** and **P-3** polymer helicity as a result of isomerization of azobenzene pendants with the random distribution of **M-2** throughout the polymer backbone. During the polymerization, a small amount of chiral stimulant biases the helicity of the polymer which is evident from VCD (Figure S12) and SOR data. The initial SOR for the (*R*)-*N*-methyl-*N*′-phenethylcarbodiimide monomer was +48°, and the resulting polymers **P-2** and **P-3** showed oppositely signed SOR of −113° and −156°, respectively. Thus, it is conclusive that the polymer helicity is governed by the helical backbone.[41] The homopolymer synthesized from (*R*)-*N*-methyl-*N*′-phenethylcarbodiimide monomer does not show any changes in SOR values upon UV-illumination or heating; thus, it is conclusive that changes in SOR values are solely due to dynamic isomerization of azobenzene pendants.

We attempted to induce configurational changes in the azobenzene moiety through the irradiation of polymer samples by using UV 365 nm. Photoisomerization can be induced by elevating the isomers to electronically excited states with return to the ground state through nonradiative decay. Although *trans*−*cis* isomerization of azo derivatives has been studied extensively, its precise pathway is still unclear and requires further clarification (Figure S13).[42−46]

First, we have irradiated the polymer solution with 365 nm UV light. The UV spectrum of azobenzene derivatives displays two characteristic absorption bands that correspond to $\pi-\pi^*$ (more intense band to $n-\pi^*$) transitions. We believe that the azobenzene scaffolds attached to the polymer backbone initially exist predominantly as *trans* isomers.[36] Upon irradiation with 365 nm UV light, a 360 nm peak which was observed at room temperature shifted to a shorter wavelength of 348 nm, and the intensity has been decreased due to a hypsochromic effect (blue-shift) (Figure 1). The electronic $n-\pi^*$ transition is only allowed in *cis* isomers, and the characteristic band at 448 nm is indicative of the formation of the *cis* isomer upon UV irradiation.

DOI: 10.1021/acs.macromol.8b00679
Macromolecules XXXX, XXX, XXX−XXX

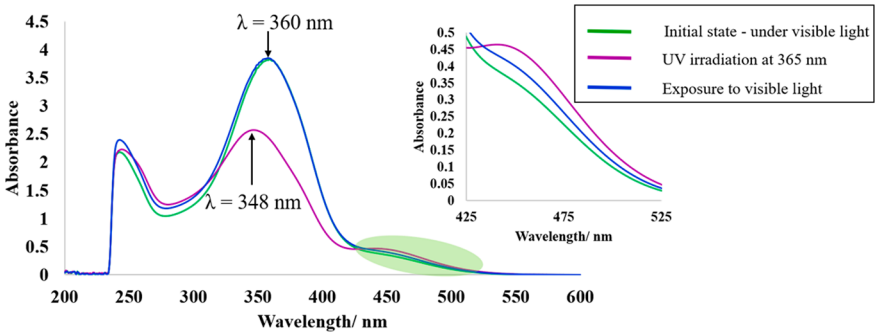

Figure 1. Overall UV−vis spectra for **P-1** with and without UV irradiation: prior to irradiation (green), after UV irradiation (purple), and removal of the source (blue). Also shown is the magnified area in the range 425−525 nm.

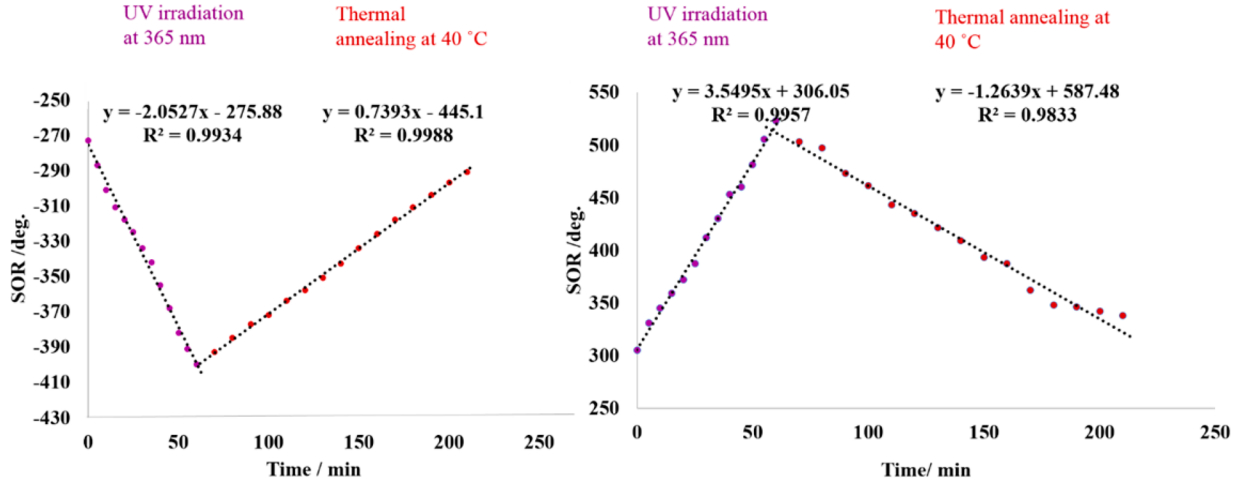

Figure 2. Change of SOR during the first cycle for (*S*)-**P-1** (left) and (*R*)-**P-1** (right) upon illumination with UV light and after removal of the light source. Note: each single data point represents the average of three consecutive readings.

To clarify the azobenzene pendant group isomerization effect on the polycarbodiimide backbone chirality, we have investigated the behavior of the **P-1**, **P-2**, and **P-3** polymers when illuminated with UV 365 nm light and subsequently exposed to visible light. The polymer samples were irradiated with 365 nm UV light, and SOR was recorded at 10 min intervals within a 1 h period. Interestingly, the SOR is linearly dependent and increasing with time; upon heating to 40 °C, it returns to the initial SOR value in a linear fashion (Figure 2). To check the reversibility, we performed simultaneous UV illumination and heating cycles, and the data clearly show that the change of SOR was reversible (Figures S14A,B). Racemization is also possible upon heating, but it seems unlikely that this would cause a change of SOR by 200° within 2 h with the temperature as low as 40 °C.

Nunzi and co-workers have reported the interesting phenomenon associated with azo-polymers, i.e., photoinduced mass movement.[47] These photoinduced movements of azopolymers have been explained by various theories and models including a diffusion model based on random walk motion,[47] thermodiffusion model,[48,49] and fluid mechanics model,[50] to name a few. Interestingly, reconfigurable azo-pendants act as a molecular machine with the polymer material mass migration being driven by the isomerization process.[51] The isomerization of the azo-pendant groups can induce spring-like contraction and expansion movements. We believe that such UV-triggered reconfigurations generate a photoisomerization force which imparts changes to the helical backbone. Indeed, the Stupp lab ascribed the change of the helical pitch of nanofibers exposed to UV light to the isomerization process.[52] Specifically, in the study from the Stupp lab the *cis* isomer possesses less planarity than the corresponding *trans* isomer, increasing sterically induced torque on the backbone which leads to a low chiral pitch. Similarly, azobenzene decorated polycarbodiimides show configurational changes under UV illumination consistent with expansion−contraction motion of the helical backbone. This would bias the change of the helical pitch which is inferred from SOR data. However, the effect of the azobenzene pendant group isomerization appears to be insufficient to change the helicity of the backbone (helical inversion).

Molecular Dynamics Simulations. In order to gain a molecular-level picture of the effect of the azobenzene isomerization on the properties of the carbodiimide polymer, eight different systems were prepared and studied using fully atomistic molecular dynamics (MD) computer simulations. Each system, summarized in Table 1, consisted of one 80-mer under different conditions (A−H states). In each system, all 80 monomers had the same (*cis* or *trans*) conformation. The isomerization was performed instantaneously by changing the C−N−N−C torsional potential as described in the Methods section. We found a clear and dramatic difference in the polymer properties of the *cis* and *trans* conformations, independent of the other factors considered. Specifically, the *cis* isomer has a highly helical arrangement of the azobenzene pendant groups, a shorter end-to-end length, and a more compact cross section (short state). These differences are clearly seen in the

DOI: 10.1021/acs.macromol.8b00679
Macromolecules XXXX, XXX, XXX−XXX

simulation snapshots of panels A and B of Figure 3. These differences are independent of the environment (vacuum or chloroform solvent) as shown in panel A of Figure 4 for the A–D states of Table 1.

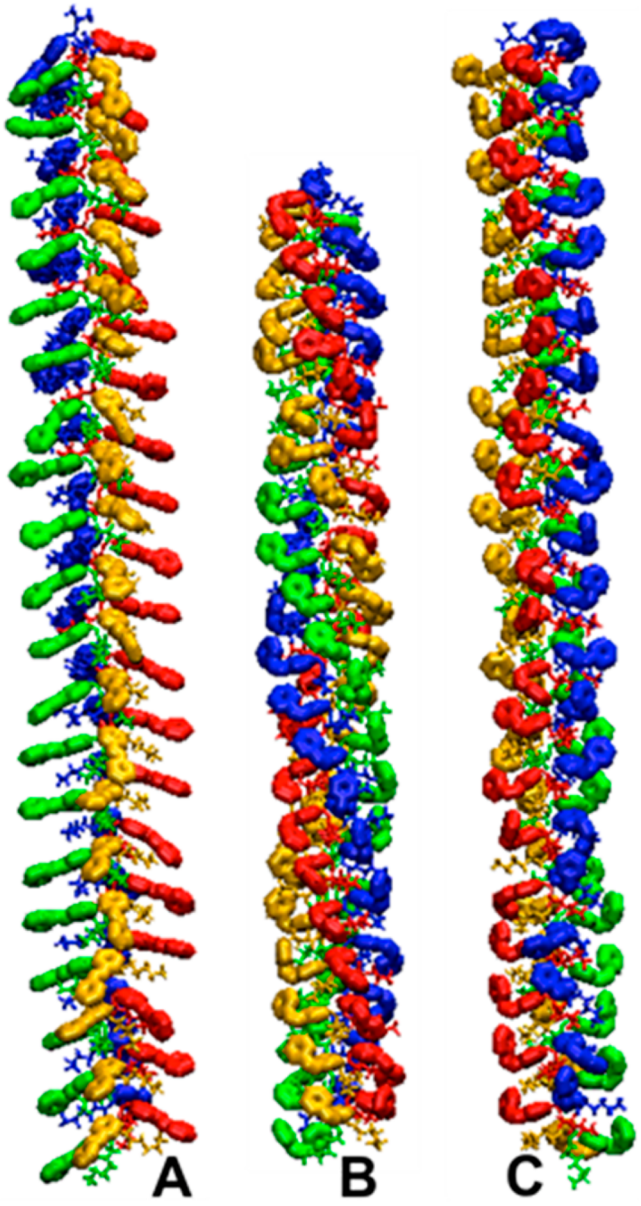

Figure 3. Representative snapshots from the MD simulations for the 80-mer (panel A) in the trans configuration and (panel B) in the *cis* configuration. Panel C shows the *cis* configuration in chloroform initiated from the "long" length which corresponds to the H state of Table 1. Monomers spaced four apart (i, i + 4) are given the same color.

Moreover, if we instantaneously change the isomer states for the A–D systems to throw them out of equilibrium, three of the four systems quickly recover (E, F, and G). For example, if we take the *cis* isomer in chloroform (blue curve in panel A of Figure 4) and change to the *trans* isomer (green curve in panel B of Figure 4), the polymer backbone elongates, becomes less helical in terms of the arrangement of the azobenzene pendant groups, and increases in cross section over a time scale of tens of nanoseconds. The only exception was the switch from *trans* to *cis* in chloroform, as shown in panel C of Figure 3 corresponding to the H state of Table 1, which does not recover to the stable *cis* state on the nanosecond time scale of the MD simulation. We hypothesize that there is a kinetic trap preventing the recovery and would expect the recovery to occur on a longer time scale.

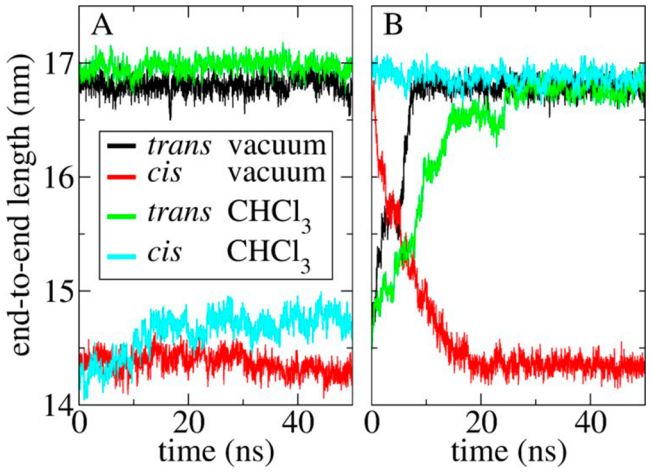

Figure 4. End-to-end length of the 80-mer over a 50 ns MD simulation under different conditions. In panel A, all of the systems are at equilibrium and correspond to the A–D states of Table 1. In panel B, all of the systems are initiated from the "wrong" length (by instantaneously changing the isomer state at the end of each A–D system simulation) and correspond to the E–H states of Table 1; the data reported in Table 1 are for the stable (plateau) region of each data set.

By combining SOR data and MD simulation studies, we can infer that upon UV illumination azobenzene pendants are confined into the *cis* configuration which induces a highly helical arrangement (Figure 3, state B-contracted helical), whereas the removal of the UV source causes the polymer backbone to elongate and become less helical (state A-elongated helical). The helicity of the polymer scaffold is more pronounced with azobenzene in its *cis* configuration (state B); thus, the polymer possesses a higher magnitude of SOR.

IR Studies. For this study, the polymer was melted by heating up to 160 °C, and the FTIR spectra were recorded while cooling and during a second heating cycle. Under thermal annealing conditions, we mainly focus on three important regions in the FTIR spectrum which is associated with 1100–1250 cm^{-1} (C–N stretch), around 1400 cm^{-1} (N=N stretches), and 1620–1680 cm^{-1} which corresponds to the imine (C=N stretches) (Figure 5A, Figures S17–S20). To make a better comparison, we utilized DFT calculated IR spectra to distinguish the main changes for the *cis* isomer. Using DFT, we computed the IR spectra of eight model octamers whose initial structures were based on the fragments of the 80-mer MD structures (Figure 3A,B, Figures S15 and S16). The calculated IR spectra (Figure 5B) agree well with the experimental data, and the DFT normal modes mostly support peak assignments of the experimental FTIR spectra. Particularly, C=N stretches are found from 1590 to 1700 cm^{-1}, N=N stretches are at 1400–1480 cm^{-1}, and C–N and $C_{aromatic}$–N stretches are from 1100 to 1400 cm^{-1}. Distinct differences between the *cis* and *trans* spectra are observed in the following areas which match the experimental results.

First, as temperature increases, a new peak is observed at 1678 cm^{-1} which corresponds to C=N imine stretch. This peak appears due to changes in the polymer backbone.

DOI: 10.1021/acs.macromol.8b00679
Macromolecules XXXX, XXX, XXX–XXX

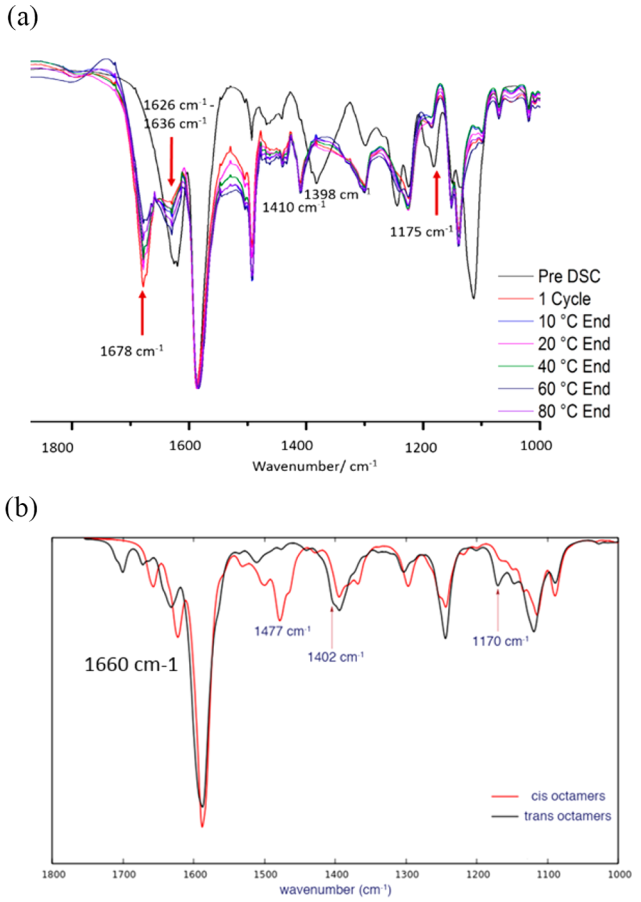

Figure 5. (a) FTIR spectra for **P-1** under thermal annealing. (b) DFT calculated IR spectra for *cis* and *trans* octamers. Each spectrum is an average of the spectra of the four conformations for each state.

Interestingly, the intensity of the peak at 1678 cm^{-1} decreases while the band at 1636 cm^{-1} increases with increasing temperature. DFT computed IR spectra also showed a new peak at 1660 cm^{-1} for the *cis* isomer which validates the configurational changes. The same experiment was performed on poly(*N*-phenyl-*N*′-hexylcarbodiimide) as a control; the FTIR spectra did not show any significant changes in the imine region (Figure S21). Therefore, we believe that the reconfiguration of the azo bond (N═N) appended to the helical backbone induces changes in the polymer main chain geometry upon thermal annealing.

Second, the peak ascribed to the N═N (azo bond) originally at 1398 cm^{-1} shifts to 1420 cm^{-1}. This peak at a higher stretching frequency may be related to the dipole moment generated in the *cis* isomer. In the DFT model, the N═N stretch modes were identified at 1402 cm^{-1} for the *trans* isomer and shifted to a higher frequency of 1477 cm^{-1} for the *cis* isomer. This shift is consistent with the experimental observations though with some discrepancy for the peak positions of the *cis* isomer.

Furthermore, a peak at 1170 cm^{-1} is present only in the *trans* isomer spectra obtained from DFT modeling, and the normal mode of this peak indicates stretching along the linear benzene−N═N−benzene motif, which is absent in the *cis* state. On the experimental FTIR spectra, a peak at 1170 cm^{-1} is also dominant for the *trans* state. In summary, DFT calculations corroborated the experimental and MD simulation results on the *cis*−*trans* conformational changes.

Polymer Thin Film Topology Studies by Using TM-AFM. The polymer topology in a thin film has been inspected by using TM-AFM to reveal photoinduced surface deformation under UV light. This phenomenon takes place due to mass movement of the polymer scaffolds which is fueled by dynamic photoisomerization of the azobenzene chromophore. The phenomenology of photomigration was witnessed from experimental work that azopolymers display photofluidic motions upon isomerization process.[51,53,54] The contraction−expansion helical movements are attributed to the 3-dimentional space translational motions which lead to changes in the position of polymeric chains. We have investigated the topology of polymer thin films both in $C_2H_2Cl_4$ (1,1,2,2-tetrachloroethane) (Figure S22A) and $CHCl_3$ solvents (Figure S22B). We believe that these changes in polymer roughness occur due to a photomigration effect. The surface smoothing effect observed for both **P-1** and **P-2** is probably associated with this phenomenon due to the more isotropic shape of the *cis* configuration. In **P-3**, when casting from $C_2H_2Cl_4$, surface smoothing was unremarkable due to the high content of chiral monomer in random copolymer structure. When $CHCl_3$ was used, irregularly shaped aggregations were found under UV illumination, and there are no significant changes in surface properties. In general, SEM observations (Figure S23) support the AFM findings showing smoothing of the surface of the polymer after exposure to UV light.

Lyotropic Liquid Crystalline Behavior. Azobenzene conjugated molecules can undergo liquid crystalline phase transitions under UV illumination.[55−57] Specifically, the *trans* to *cis* isomerization due to UV light changes the azobenzene configuration into a bent shape and this nonmesogenic nature interrupts the liquid crystalline order.[5] Moreover, liquid crystalline materials can be doped with photoresponsive compounds, and phase transitions can occur because of changes in helical pitch.[58] This contributes to alterations of its chirality through the manipulation of cholesteric pitch. By keeping in mind these previously reported liquid crystalline behaviors of azobenzene-decorated materials, we have investigated liquid crystalline properties of (*S*) family of 12.3% (w/w) of **P-1**, **P-2**, and **P-3** in chloroform.[59,60] We have observed that prior to UV illumination, all three polymers showed nematic liquid crystalline domains whereas the ordered liquid crystalline phase was disrupted upon the triggering event (Figure S24). These changes occurred due to the formation of the nonmesogenic, bent-shaped *cis* isomer under UV illumination.[5,19] Thus, the incorporation of rod-like *trans*-azobenzene pendants into polycarbodiimides causes liquid crystalline behavior, whereas the induced bent-shaped *cis* configuration disrupts the packing tendency.[61,62] Further, these POM findings complement our AFM and SEM data showing enhance structural uniformity and smoothness of the surface upon UV irradiation of the polymer material.

CONCLUSIONS

Azobenzene-decorated polycarbodiimides have been synthesized via screw sense polymerization with chiral BINOL initiators and chiral stimulant through the sergeants-and-soldiers effect. The isomerization of the azobenzene chromophore appended on the helical backbone takes place under illumination with UV 365 nm light in solution. Fully atomistic molecular dynamics computer simulations together with chiral studies demonstrate that these polymers display spring-like expansion−contraction motion under UV irradiation. In the solid state,

DOI: 10.1021/acs.macromol.8b00679
Macromolecules XXXX, XXX, XXX−XXX

FTIR experiments revealed that changes in the helical backbone occurred as a result of the isomerization process upon thermal annealing at 120 °C, and the IR spectra computed from DFT calculations displayed good agreement for *trans*−*cis* isomerization. Phenomenologically, we demonstrated for the first time that photoisomerization and the closely related process of photomigration of azobenzene-decorated polycarbodiimide scaffolds may change the thin film surface roughness as evidenced by a combination of AFM, SEM, and POM techniques. This type of reconfigurable polymeric molecular switch can advance many areas of applied research, which may result in the emergence of unique polymeric materials including chiral sensors, drug delivery systems, photovoltaics, and optical tweezers.

■ ASSOCIATED CONTENT

Supporting Information

The Supporting Information is available free of charge on the ACS Publications website at DOI: 10.1021/acs.macromol.8b00679.

Experimental procedures for the synthesis of all monomers, and polymers, along with the corresponding NMR, IR, computational data, *p*-XRD profiles, AFM, and SEM (PDF)

Helical contraction−expansion: *cis* long to short—a change of azobenzene configuration from *cis* long state to short state (MPG)

Helical contraction−expansion: *trans* short to long—a change of azobenzene configuration from *trans* configuration change from short state to long state (MPG)

■ AUTHOR INFORMATION

Corresponding Authors

*E-mail: Bruce.novak@utdallas.edu (B.M.N.).
*E-mail: dxs124830@utdallas.edu (D.A.S.).

ORCID

Dumindika A. Siriwardane: 0000-0001-9978-9651
Steven O. Nielsen: 0000-0003-3390-3313

Funding

Funding for this was provide by Faculty start-up fund from The University of Texas at Dallas (UTD).

Notes

The authors declare no competing financial interest.

■ ACKNOWLEDGMENTS

We gratefully acknowledge the NSF-MRI grant (CHE-1126177) used to purchase the Bruker Advance III 500 NMR instrument.

■ REFERENCES

(1) Kennemur, J. G.; Kilgore, C. A.; Novak, B. M. Adjusting conformational switching behavior of helical polycarbodiimides through substituent induced polarity effects. *J. Polym. Sci., Part A: Polym. Chem.* **2011**, *49* (3), 719−728.

(2) Zarzar, L. D.; Sresht, V.; Sletten, E. M.; Kalow, J. A.; Blankschtein, D.; Swager, T. M. Dynamically reconfigurable complex emulsions via tunable interfacial tensions. *Nature* **2015**, *518*, 520.

(3) Dinçalp, H.; Yavuz, S.; Haklı, Ö.; Zafer, C.; Özsoy, C.; Durucasu, İ.; İçli, S. *J. Photochem. Photobiol., A* **2010**, *210*, 8−16.

(4) Ge, F.; Zhao, Y. A new function for thermal phase transition-based polymer actuators: autonomous motion on a surface of constant temperature †Electronic supplementary information (ESI) available: Additional figures, tables, discussions and experimental information. See DOI: 10.1039/C7SC01792H Click here for additional data file. Click here for additional data file. Click here for additional data file. *Chemical Science* **2017**, *8* (9), 6307−6312.

(5) Lin, H.; Xiao, W.; Qin, S.-Y.; Cheng, S.-X.; Zhang, X.-Z. Switch on/off microcapsules for controllable photosensitive drug release in a 'release-cease-recommence' mode. *Polym. Chem.* **2014**, *5* (15), 4396.

(6) Serra, F.; Terentjev, E. M. Effects of Solvent Viscosity and Polarity on the Isomerization of Azobenzene. *Macromolecules* **2008**, *41* (3), 981−986.

(7) Asano, T.; Okada, T. Thermal Z-E isomerization of azobenzenes. The pressure, solvent, and substituent effects. *J. Org. Chem.* **1984**, *49* (23), 4387−4391.

(8) Wei, F.; Ye, S. Molecular-Level Insights into N−N π-Bond Rotation in the pH-Induced Interfacial Isomerization of 5-Octadecyloxy-2-(2-pyridylazo)phenol Monolayer Investigated by Sum Frequency Generation Vibrational Spectroscopy. *J. Phys. Chem. C* **2012**, *116* (31), 16553−16560.

(9) Norikane, Y.; Tamaoki, N. Light-Driven Molecular Hinge: A New Molecular Machine Showing a Light-Intensity-Dependent Photoresponse that Utilizes the Trans−Cis Isomerization of Azobenzene. *Org. Lett.* **2004**, *6* (15), 2595−2598.

(10) Jiang, S.; Zhao, Y.; Wang, L.; Yin, L.; Zhang, Z.; Zhu, J.; Zhang, W.; Zhu, X. Photocontrollable induction of supramolecular chirality in achiral side chain Azo-containing polymers through preferential chiral solvation. *Polym. Chem.* **2015**, *6* (23), 4230−4239.

(11) Lin, T.-H.; Jau, H.-C.; Hung, S.-Y.; Fuh, H.-R.; Fuh, A. Y.-G. Photoaddressable bistable reflective liquid crystal display. *Appl. Phys. Lett.* **2006**, *89* (2), 021116.

(12) Liu, J.-H.; Wang, H.-Y. Optical switching behavior of polymer-dispersed liquid crystal composite films with various novel azobenzene derivatives. *J. Appl. Polym. Sci.* **2004**, *91* (2), 789−799.

(13) Kundu, S.; Kang, S.-W. Photo-stimulated phase and anchoring transitions of chiral azo-dye doped nematic liquid crystals. *Opt. Express* **2013**, *21* (25), 31324−31329.

(14) Bergbreiter, D. E.; Osburn, P. L.; Li, C. Soluble Polymer-Supported Catalysts Containing Azo Dyes. *Org. Lett.* **2002**, *4* (5), 737−740.

(15) Van Den Mooter, G.; Maris, B.; Samyn, C.; Augustijns, P.; Kinget, R. Use of azo polymers for colon-specific drug delivery. *J. Pharm. Sci.* **1997**, *86* (12), 1321−1327.

(16) Merten, C.; Reuther, J. F.; DeSousa, J. D.; Novak, B. M. Identification of the specific, shutter-like conformational reorientation in a chiroptical switching polycarbodiimide by VCD spectroscopy. *Phys. Chem. Chem. Phys.* **2014**, *16* (23), 11456−11460.

(17) Zarzar, L. D.; Sresht, V.; Sletten, E. M.; Kalow, J. A.; Blankschtein, D.; Swager, T. M. Dynamically reconfigurable complex emulsions via tunable interfacial tensions. *Nature* **2015**, *518* (7540), 520−524.

(18) Mochida, Y.; Cabral, H.; Miura, Y.; Albertini, F.; Fukushima, S.; Osada, K.; Nishiyama, N.; Kataoka, K. Bundled Assembly of Helical Nanostructures in Polymeric Micelles Loaded with Platinum Drugs Enhancing Therapeutic Efficiency against Pancreatic Tumor. *ACS Nano* **2014**, *8* (7), 6724−6738.

(19) Jha, S. K.; Cheon, K.-S.; Green, M. M.; Selinger, J. V. Chiral Optical Properties of a Helical Polymer Synthesized from Nearly Racemic Chiral Monomers Highly Diluted with Achiral Monomers. *J. Am. Chem. Soc.* **1999**, *121* (8), 1665−1673.

(20) Maxein, G.; Zentel, R. Photochemical Inversion of the Helical Twist Sense in Chiral Polyisocyanates. *Macromolecules* **1995**, *28* (24), 8438−8440.

(21) Sahl, M.; Muth, S.; Branscheid, R.; Fischer, K.; Schmidt, M. Helix−Coil Transition in Cylindrical Brush Polymers with Poly-l-lysine Side Chains. *Macromolecules* **2012**, *45* (12), 5167−5175.

(22) Ciardelli, F.; Fabbri, D.; Pieroni, O.; Fissi, A. Photomodulation of polypeptide conformation by sunlight in spiropyran-containing poly(L-glutamic acid). *J. Am. Chem. Soc.* **1989**, *111* (9), 3470−3472.

(23) Yu, Z.; Hecht, S. Remote control over folding by light. *Chem. Commun.* **2016**, *52* (40), 6639−6653.

DOI: 10.1021/acs.macromol.8b00679
Macromolecules XXXX, XXX, XXX−XXX

(24) Murugesan, M.; Abbineni, G.; Nimmo, S. L.; Cao, B.; Mao, C. Virus-based Photo-Responsive Nanowires Formed By Linking Site-Directed Mutagenesis and Chemical Reaction. *Sci. Rep.* **2013**, *3*, 1820.
(25) Renner, C.; Moroder, L. Azobenzene as Conformational Switch in Model Peptides. *ChemBioChem* **2006**, *7* (6), 868−878.
(26) Mart, R. J.; Allemann, R. K. Azobenzene photocontrol of peptides and proteins. *Chem. Commun.* **2016**, *52* (83), 12262−12277.
(27) Rananaware, A.; Samanta, M.; Bhosale, R. S.; Kobaisi, M. A.; Roy, B.; Bheemireddy, V.; Bhosale, S. V.; Bandyopadhyay, S.; Bhosale, S. V. Photomodulation of fluoride ion binding through anion-π interactions using a photoswitchable azobenzene system. *Sci. Rep.* **2016**, *6*, 22928.
(28) Beharry, A. A.; Wong, L.; Tropepe, V.; Woolley, G. A. Fluorescence Imaging of Azobenzene Photoswitching In Vivo. *Angew. Chem., Int. Ed.* **2011**, *50* (6), 1325−1327.
(29) Phillips, J. C.; Braun, R.; Wang, W.; Gumbart, J.; Tajkhorshid, E.; Villa, E.; Chipot, C.; Skeel, R. D.; Kalé, L.; Schulten, K. Scalable molecular dynamics with NAMD. *J. Comput. Chem.* **2005**, *26* (16), 1781−1802.
(30) Vanommeslaeghe, K.; MacKerell, A. D. Automation of the CHARMM General Force Field (CGenFF) I: Bond Perception and Atom Typing. *J. Chem. Inf. Model.* **2012**, *52* (12), 3144−3154.
(31) Vanommeslaeghe, K.; Raman, E. P.; MacKerell, A. D. Automation of the CHARMM General Force Field (CGenFF) II: Assignment of Bonded Parameters and Partial Atomic Charges. *J. Chem. Inf. Model.* **2012**, *52* (12), 3155−3168.
(32) Böckmann, M.; Peter, C.; Site, L. D.; Doltsinis, N. L.; Kremer, K.; Marx, D. Atomistic Force Field for Azobenzene Compounds Adapted for QM/MM Simulations with Applications to Liquids and Liquid Crystals. *J. Chem. Theory Comput.* **2007**, *3* (5), 1789−1802.
(33) Yin, C.-C.; Li, A. H.-T.; Chao, S. D. Liquid chloroform structure from computer simulation with a full ab initio intermolecular interaction potential. *J. Chem. Phys.* **2013**, *139* (19), 194501.
(34) Humphrey, W.; Dalke, A.; Schulten, K. VMD: Visual molecular dynamics. *J. Mol. Graphics* **1996**, *14* (1), 33−38.
(35) Frisch, M. J.; Trucks, G. W.; Schlegel, H. B.; Scuseria, G. E.; Robb, M. A.; Cheeseman, J. R.; Scalmani, G.; Barone, V.; Mennucci, B.; Petersson, G. A.; Nakatsuji, H.; Caricato, M.; Li, X.; Hratchian, H. P.; Izmaylov, A. F.; Bloino, J.; Zheng, G.; Sonnenberg, J. L.; Hada, M.; Ehara, M.; Toyota, K.; Fukuda, R.; Hasegawa, J.; Ishida, M.; Nakajima, T.; Honda, Y.; Kitao, O.; Nakai, H.; Vreven, T.; Montgomery, Jr., J. A.; Peralta, J. E.; Ogliaro, F.; Bearpark, M.; Heyd, J. J.; Brothers, E.; Kudin, K. N.; Staroverov, V. N.; Keith, T.; Kobayashi, R.; Normand, J.; Raghavachari, K.; Rendell, A.; Burant, J. C.; Iyengar, S. S.; Tomasi, J.; Cossi, M.; Rega, N.; Millam, J. M.; Klene, M.; Knox, J. E.; Cross, J. B.; Bakken, V.; Adamo, C.; Jaramillo, J.; Gomperts, R.; Stratmann, R. E.; Yazyev, O.; Austin, A. J.; Cammi, R.; Pomelli, C.; Ochterski, J. W.; Martin, R. L.; Morokuma, K.; Zakrzewski, V. G.; Voth, G. A.; Salvador, P.; Dannenberg, J. J.; Dapprich, S.; Daniels, A. D.; Farkas, O.; Foresman, J. B.; Ortiz, J. V.; Cioslowski, J.; Fox, D. J. *Gaussian 09*, Revision D.01; Gaussian, Inc.: Wallingford, CT, 2013.
(36) Scalmani, G.; Frisch, M. J. Continuous surface charge polarizable continuum models of solvation. I. General formalism. *J. Chem. Phys.* **2010**, *132* (11), 114110.
(37) Budhathoki-Uprety, J.; Novak, B. M. Synthesis of Alkyne-Functionalized Helical Polycarbodiimides and their Ligation to Small Molecules using 'Click' and Sonogashira Reactions. *Macromolecules* **2011**, *44* (15), 5947−5954.
(38) Budhathoki-Uprety, J.; Peng, L.; Melander, C.; Novak, B. M. Synthesis of Guanidinium Functionalized Polycarbodiimides and Their Antibacterial Activities. *ACS Macro Lett.* **2012**, *1* (3), 370−374.
(39) Reuther, J. F.; Novak, B. M. Evidence of Entropy-Driven Bistability through 15N NMR Analysis of a Temperature- and Solvent-Induced, Chiroptical Switching Polycarbodiimide. *J. Am. Chem. Soc.* **2013**, *135* (51), 19292−19303.
(40) Green, M. M.; Reidy, M. P.; Johnson, R. D.; Darling, G.; O'Leary, D. J.; Willson, G. Macromolecular stereochemistry: the out-of-proportion influence of optically active comonomers on the conformational characteristics of polyisocyanates. The sergeants and soldiers experiment. *J. Am. Chem. Soc.* **1989**, *111* (16), 6452−6454.
(41) Siriwardane, D. A.; Kulikov, O.; Reuther, J. F.; Novak, B. M. Rigid, Helical Arm Stars through Living Nickel Polymerization of Carbodiimides. *Macromolecules* **2017**, *50* (3), 832−840.
(42) Merino, E.; Ribagorda, M. Control over molecular motion using the cis−trans photoisomerization of the azo group. *Beilstein J. Org. Chem.* **2012**, *8*, 1071−1090.
(43) Bandara, H. M. D.; Burdette, S. C. Photoisomerization in different classes of azobenzene. *Chem. Soc. Rev.* **2012**, *41* (5), 1809−1825.
(44) Tiberio, G.; Muccioli, L.; Berardi, R.; Zannoni, C. How Does the Trans−Cis Photoisomerization of Azobenzene Take Place in Organic Solvents? *ChemPhysChem* **2010**, *11* (5), 1018−1028.
(45) Le Fevre, R. J. W.; Northcott, J. 178. The effects of substituents and solvents on the cis[rightward arrow]trans change of azobenzene. *J. Chem. Soc.* **1953**, *0*, 867−870.
(46) Shinkai, S.; Kusano, Y.; Shigematsu, K.; Manabe, O. *Chem. Lett.* **1980**, *9*, 1303−1306.
(47) Lefin, P.; Fiorini, C.; Nunzi, J.-M. Anisotropy of the photo-induced translation diffusion of azobenzene dyes in polymer matrices. *Pure Appl. Opt.* **1998**, *7* (1), 71.
(48) Garcia-Amoros, J.; Velasco, D. Understanding the fast thermal isomerisation of azophenols in glassy and liquid-crystalline polymers. *Phys. Chem. Chem. Phys.* **2014**, *16* (7), 3108−3114.
(49) Voit, A.; Krekhov, A.; Enge, W.; Kramer, L.; Köhler, W. Thermal Patterning of a Critical Polymer Blend. *Phys. Rev. Lett.* **2005**, *94* (21), 214501.
(50) Sumaru, K.; Yamanaka, T.; Fukuda, T.; Matsuda, H. Photoinduced surface relief gratings on azopolymer films: Analysis by a fluid mechanics model. *Appl. Phys. Lett.* **1999**, *75* (13), 1878−1880.
(51) Sekkat, Z. Optical tweezing by photomigration. *Appl. Opt.* **2016**, *55* (2), 259−268.
(52) Li, L.-s.; Jiang, H.; Messmore, B. W.; Bull, S. R.; Stupp, S. I. A Torsional Strain Mechanism To Tune Pitch in Supramolecular Helices. *Angew. Chem., Int. Ed.* **2007**, *46* (31), 5873−5876.
(53) Karageorgiev, P.; Neher, D.; Schulz, B.; Stiller, B.; Pietsch, U.; Giersig, M.; Brehmer, L. From anisotropic photo-fluidity towards nanomanipulation in the optical near-field. *Nat. Mater.* **2005**, *4*, 699.
(54) Lee, S.; Kang, H. S.; Park, J.-K. Directional Photofluidization Lithography: Micro/Nanostructural Evolution by Photofluidic Motions of Azobenzene Materials. *Adv. Mater.* **2012**, *24* (16), 2069−2103.
(55) Wang, Y.; Li, Q. Light-Driven Chiral Molecular Switches or Motors in Liquid Crystals. *Adv. Mater.* **2012**, *24* (15), 1926−1945.
(56) Rahman, M. L.; Hegde, G.; Azazpour, M.; Yusoff, M. M.; Kumar, S. Synthesis and characterization of liquid crystalline azobenzene chromophores with fluorobenzene terminal. *J. Fluorine Chem.* **2013**, *156*, 230−235.
(57) Ichimura, K. Photoalignment of Liquid-Crystal Systems. *Chem. Rev.* **2000**, *100* (5), 1847−1874.
(58) Iamsaard, S.; Bosco, A.; Cornelissen, J. J. L. M.; Feringa, B. L.; Katsonis, N. Time-programmed helix inversion in phototunable liquid crystals. *Chem. Commun.* **2013**, *49* (39), 4256−4258.
(59) Kim, J.; Novak, B. M.; Waddon, A. J. Lyotropic Liquid Crystalline Properties of Poly(N,N′-di-n-hexylguanidine). *Macromolecules* **2004**, *37* (4), 1660−1662.
(60) Xue, Q.; Kimura, T.; Fukuda, T.; Shimada, S.; Matsuda, H. Synthesis and lyotropic liquid crystal properties of chiral helical polycarbodiimides. *Liq. Cryst.* **2004**, *31* (2), 137−143.
(61) Poutanen, M.; Ikkala, O.; Priimagi, A. Structurally Controlled Dynamics in Azobenzene-Based Supramolecular Self-Assemblies in Solid State. *Macromolecules* **2016**, *49* (11), 4095−4101.
(62) Yu, H.; Ikeda, T. Photocontrollable Liquid-Crystalline Actuators. *Adv. Mater.* **2011**, *23* (19), 2149−2180.

DOI: 10.1021/acs.macromol.8b00679
Macromolecules XXXX, XXX, XXX−XXX